Interhelical Interactions in the gp41 Core: Implications for Activation of HIV-1 Membrane Fusion†,‡

Shilong Wang,§ Joanne York,|| Wei Shu,§ Marisa O. Stoller,|| Jack H. Nunberg,*,|| and Min Lu*,§

Department of Biochemistry, Weill Medical College of Cornell University, New York, New York 10021, and Montana Biotechnology Center, The University of Montana, Missoula, Montana 59812

Received February 7, 2002; Revised Manuscript Received March 29, 2002

ABSTRACT: The human immunodeficiency virus type 1 (HIV-1) envelope glycoprotein complex (gp120−gp41) promotes viral entry by mediating the fusion of viral and cellular membranes. Formation of a stable trimer-of-hairpins structure in the gp41 ectodomain brings the two membranes into proximity, leading to membrane fusion. The core of this hairpin structure is a six-helix bundle in which three carboxyl-terminal outer helices pack against an inner trimeric coiled coil. Here we investigate the role of these conserved interhelical interactions on the structure and function of both the envelope glycoprotein and the gp41 core. We have replaced each of the eight amino acids at the buried face of the carboxyl-terminal helix with a representative amino acid, alanine. Structural and physicochemical characterization of the alanine mutants shows that hydrophobic interactions are a dominant factor in the stabilization of the six-helix bundle. Alanine substitutions at the Trp628, Trp631, Ile635, and Ile642 residues also affected envelope processing and/or gp120−gp41 association and abrogated the ability of the envelope glycoprotein to mediate cell−cell fusion. These results suggest that the amino-terminal region of the gp41 outer-layer α-helix plays a key role in the sequence of events associated with HIV-1 entry and have implications for the development of antibodies and small-molecule inhibitors of this conserved element.

Entry of human immunodeficiency virus type 1 (HIV-1)[1] into target cells requires the fusion of viral and cellular membranes, a process mediated by the viral envelope glycoprotein in conjunction with receptors on the host cell. The HIV-1 envelope glycoprotein is initially synthesized as the polyprotein precursor gp160, which is glycosylated and oligomerizes in the rough endoplasmic reticulum, and is then proteolytically cleaved into two subunits by furin-like enzymes in the Golgi network (*1*, *2*). The resulting surface (gp120) and transmembrane (gp41) subunits remain non-covalently associated and are translocated to the cell membrane for incorporation into budding virions. Infection is initiated by binding of gp120 to the cell-surface receptor CD4 and to one of several coreceptors (members of the chemokine receptor family) (*3*−*5*). This receptor binding induces a series of conformational changes in the envelope glycoprotein, leading to exposure of the hydrophobic N-terminal fusion peptide of the gp41 ectodomain and the initiation of membrane fusion events (*6*−*8* and references therein). An understanding of this fusion activation process is important for elucidation of viral entry mechanisms and development of immunologic and pharmacologic strategies for preventing HIV-1 infection.

The ectodomain of gp41 contains two α-helical regions, one adjacent to the N-terminal fusion peptide and one near the C-terminal transmembrane segment (*9*−*11*). Biophysical and structural analyses indicate that these two helical regions associate to form a highly stable six-helix bundle in which a central trimeric coiled coil formed by the N-terminal helical region of gp41 is surrounded by three antiparallel C-terminal helices that bind to conserved hydrophobic grooves on the coiled-coil surface (*12*−*15*). Residues at positions *a* and *d* (the first and fourth residues of the heptad repeat, respectively) of the C-terminal helix pack against residues at the *e* and *g* positions of the N-terminal coiled-coil trimer. This six-helix bundle represents the core of the fusion-active gp41 trimer-of-hairpins conformation (*12*, *16*, *17*). The hairpin structure is thought to bring the virus and cell membranes into proximity and thereby to facilitate the fusion of the two bilayers (*14*, *18*−*20*). The large body of evidence suggests that gp41 likely exists in at least three conformations: (i) a metastable prefusogenic state, which is stabilized by extensive interactions with the gp120 subunit, (ii) a "prehairpin" intermediate, formed by exposure of the fusion peptide region and concurrent formation of the N-terminal coiled coil (*19*, *21*, *22*), and (iii) the fusogenic trimer-of-hairpins form, where the C-terminal helix associates with the N-terminal coiled

† This work was supported by National Institutes of Health Grants AI44669 to J.H.N. and AI48385 to M.L. J.H.N. is also grateful to the J. B. Pendleton Charitable Trust for their support.

‡ Atomic coordinates have been deposited in the Protein Data Bank (entries 1K33 and 1K34).

* To whom correspondence should be addressed. M.L.: phone, (212) 746-6562; fax, (212) 746-8875; e-mail, mlu@mail.med.cornell.edu. J.H.N.: phone, (406) 243-6421; fax, (406) 243-6425; e-mail, nunberg@selway.umt.edu.

§ Weill Medical College of Cornell University.

|| University of Montana.

[1] Abbreviations: HIV-1, human immunodeficiency virus type 1; SIV, simian immunodeficiency virus; $[\theta]_{222}$, molar ellipticity at 222 nm; CD, circular dichroism; HPLC, high-performance liquid chromatography; T_m, midpoint of thermal denaturation; GdmCl, guanidinium hydrochloride; PBS, neutral pH phosphate-buffered saline; PDB, Protein Data Bank; rms, root-mean-square; HIVIG, anti-HIV immunoglobulin from infected persons; PAGE, polyacrylamide gel electrophoresis; mAb, monoclonal antibody; HRP, horseradish peroxidase.

10.1021/bi025648y CCC: $22.00
Published on Web 05/10/2002

coil to induce membrane apposition and fusion. Formation of the gp41 hairpin structure is likely to be an important thermodynamic driving force for the conformational activation of the envelope glycoprotein (*23*).

Peptides derived from the N- and C-terminal helical regions of the gp41 ectodomain (termed N-peptides and C-peptides, respectively) are potent inhibitors of HIV-1 infection and syncytium formation (*24*, *25*). The C-peptide T-20 has been shown in human clinical trials to be effective in suppressing HIV-1 replication (*26*). The available evidence indicates that C-peptides inhibit formation of the fusogenic six-helix bundle in a dominant-negative manner by binding to the transiently exposed N-terminal coiled coil in the prehairpin intermediate (*12*, *19*, *22*, *27*, *28*). Consistent with this notion, replacement of a conserved glutamine (Gln652) in the C-helix with leucine strengthens interhelical packing interactions in the gp41 core and also increases the antiviral potency of the corresponding C-peptide (*29*). In addition, recent work has shown that a hydrophobic pocket on the surface of the N-terminal coiled coil is a potential target for the development of small-molecule HIV-1 entry inhibitors (*30*−*32*). In the gp41 core structure, this pocket is filled by three residues from the C-helix (Trp628, Trp631, and Ile635) (*13*−*15*). Mutagenesis studies indicate that these bulky hydrophobic residues contribute to the stability of the gp41 core and to the inhibitory activity of C-peptides (*33*). Taken together, these results suggest that interhelix interactions in the fusogenic hairpin structure may serve as the basis for the design of a new class of antiviral agents.

In this study, we have performed a systematic analysis of the role of individual side chains at positions *a* and *d* of the gp41 outer-layer C-helix in determining the structure and function of the HIV-1 envelope glycoprotein. Our results show that the six-helix bundle structure is largely stabilized through specific interfacial interactions between six buried apolar side chains (Trp628, Trp631, Ile635, Tyr638, Ile642, and Leu645) and is destabilized by two buried polar residues (Ser649 and Gln652). Alanine substitutions at four of these bulky hydrophobic residues (Trp628, Trp631, Ile635, and Ile642) also impaired fusion function by affecting gp120−gp41 association and/or gp160 processing. Our studies demonstrate the critical role of the N-terminal region of the gp41 C-helix in HIV-1-mediated fusion events. This conserved element may be a useful target for the development of antibodies and small-molecule inhibitors for the treatment of HIV-1 infection.

MATERIALS AND METHODS

Peptide Expression and Purification. Alanine substitutions were individually introduced into the HIV-1 N34(L6)C28 construct by using the method of Kunkel (*34*) and verified by DNA sequencing. All recombinant peptides were expressed in *Escherichia coli* strain BL21(DE3)/pLysS (Novagen). Cells were grown at 37 °C in LB medium to an optical density of 0.8 at 600 nm and induced with isopropyl thio-β-D-galactoside for 3−4 h. Cells were lysed at 0 °C with glacial acetic acid. The bacterial lysate was centrifuged (35000*g* for 30 min) to separate the soluble fraction from inclusion bodies. The soluble fraction, containing the denatured gp41 core peptide, was dialyzed into 5% acetic acid overnight at room temperature. Peptides were purified from the soluble fraction to homogeneity by reverse-phase high-performance liquid chromatography (HPLC) (Waters) on a Vydac C-18 preparative column (Hesperia, CA), using a water/acetonitrile gradient in the presence of 0.1% trifluoroacetic acid, and lyophilized. The molecular weights of each peptide were confirmed by using matrix-assisted laser desorption ionization time-of-flight mass spectrometry (PerSeptive Biosystems, Framingham, MA). For all experiments, peptide stock solutions were prepared by resuspending the lyophilized peptide in water. The concentrations of the peptide stocks were determined by using tyrosine and tryptophan absorbance at 280 nm in 6 M GdmCl (*35*).

Circular Dichroism Spectroscopy. CD experiments were performed on an Aviv 62A DS circular dichroism spectrometer (Aviv Associates, Lakewood, NJ). The wavelength dependence of molar ellipticity, $[\theta]$, was monitored at 4 °C on a 10 μM peptide solution in 50 mM sodium phosphate (pH 7.0) and 100 mM NaCl (PBS) from 200 to 260 nm in a 0.1 cm path length cuvette with an averaging time of 5 s. The percent helicity was calculated by the method of Chen et al. (*36*). The thermal stability was determined by monitoring the change in the ellipticity at 222 nm as a function of temperature. Thermal melts were performed in 2 °C increments with an equilibration time of 2 min at the desired temperature and an integration time of 30 s. All melts were not reversible, and the peptide precipitated after thermal denaturation. The apparent melting temperatures, or midpoints of the cooperative thermal unfolding transitions (T_m), were determined from the maximum of the first derivative, with respect to the reciprocal of the temperature, of the $[\theta]_{222}$ values (*37*). The error in the estimation of T_m is $\pm$0.5 °C.

Sedimentation Ultracentrifugation. Sedimentation equilibrium measurements were performed on a Beckman XL-A (Beckman Coulter) analytical ultracentrifuge equipped with an An-60 Ti rotor (Beckman Coulter). Peptide solutions were dialyzed overnight against PBS (pH 7.0), loaded at initial concentrations of 10, 30, and 100 μM, and analyzed at rotor speeds at 20 000 and 23 000 rpm at 20 °C. Data sets were fitted simultaneously to a single-species model of ln(absorbance) versus (radial distance)^2 using the program NONLIN (*38*). The protein partial specific volume and solvent density were calculated as described by Laue et al. (*39*). The molecular weights of N34(L6)C28 variants, except for W631A, were all within 10% of those calculated for an ideal trimer, with no systematic deviation of the residuals.

Crystallization and Data Collection. A stock of the HPLC-purified peptide was dissolved in water, and its final peptide concentration was adjusted to 10 mg/mL. Crystals were obtained using the hanging drop method of vapor diffusion by equilibrating 2 μL drops (peptide solution mixed 1:1 with reservoir solution) against a reservoir solution at room temperature. Initial crystallization conditions were screened by using sparse matrix crystallization kits (Crystal Screen I and II, Hampton Research, Inc.) and then optimized. Primitive rhombohedral crystals of I635A were grown from 0.174 M ammonium chloride and 2% polyethylene glycol methyl ether 4000. Primitive rhombohedral crystals of I642A were obtained from 0.62 M ammonium sulfate. All crystals were transferred to a cryoprotectant solution containing 20% (v/v) glycerol in the corresponding mother liquor. Crystals were mounted in nylon loops (Hampton Research, Riverside, CA) and flash-frozen in liquid nitrogen. Diffraction data on

the I635A and I642A crystals were collected at 95 K using an R-axis IV image plate detector mounted on a Rigaku RU200 rotating anode X-ray generator at the X-ray Crystallography Facility at the Weill Medical College of Cornell University. Diffraction intensities were integrated by using DENZO and SCALEPACK software (*40*) and reduced to structural factors with the program TRUNCATE from the CCP4 program suite (*41*).

Structure Solution and Refinement. The structures of the I635A and I642A crystals were determined by molecular replacement using the program AMoRe in the CCP4 program suite (*41*, *42*). The HIV-1 N34(L6)C28 structure (entry 1STZ in the Protein Data Bank) was used as a search model. Cross-rotation and -translation functions, calculated with the search model at 15−4 Å resolution, yielded solutions for I635A (correlation coefficient = 74.1%; *R* factor = 38.1%) and I642A (correlation coefficient = 74.7%; *R* factor = 36.5%). Density interpretation and model building were carried out with the programs O and CNS (*43*, *44*). Iterative rounds of manual rebuilding and refinement increased the quality of the initial electron density maps and served to reduce model bias, as guided chiefly by improvement in the free *R* factor. Crystallographic refinements were carried out with the program CNS 1.0 (*45*). Since molecular replacement methods can cause a final model to be biased by the search model, the current I635A and I642A models were verified by simulated annealing omit maps. The quality of coordinates was examined by PROCHECK (*46*). All the amino acids were in the most favored regions of the Ramachandran plot. Residues Ala578, Arg579, Glu654, and Lys655 of I635A and Ser546, Arg579, Glu654, and Lys655 of I642A were left out of the model because of the absence of interpretable electron density for these atoms. The side chains of Ser546, as well as Ile548, Gln652, and Gln653, of I635A are disordered and were thus modeled as glycine and alanine, respectively. The side chains of Gln550 and Gln652, as well as Gln567, of I642A were modeled as serine and alanine, respectively.

Transfections and Envelope Glycoprotein Expression. Alanine mutations were introduced into the HXB2 envelope glycoprotein by using QuikChange mutagenesis (Stratagene, La Jolla, CA) and confirmed by DNA sequencing. A proviral fragment containing the HXB2 *rev* and *env* genes was subcloned into the eukaryotic expression plasmid pCR-Uni 3.1 (Invitrogen) as described previously (*47*, *48*). Approximately 6×10^5 COS-7 cells were plated in a 6 cm culture dish 1 day prior to transfection. A half-microgram of envelope glycoprotein expression plasmid and 2.5 μg of the pcDNA3.1 vector (Invitrogen) were cotransfected with the FuGene-6 reagent (Roche Molecular Biochemicals). After incubation for 18 h at 37 °C, the cells were washed with Dulbecco's phosphate-buffered saline and then re-fed with Dulbecco's modified Eagle's medium containing 10% fetal bovine serum. The cultures were continued at 37 °C for 24 h before harvesting for cell−cell fusion assays or for Western blot analysis.

Envelope glycoprotein expression in transfected cells was assayed by Western blot analysis as previously described (*48*). Briefly, to detect soluble gp120 in culture medium, the cell supernatants were filtered, and shed gp120 was immunoprecipitated by using anti-HIV immunoglobulin from infected persons (HIVIG) (*49*) and the Protein A−Sepharose conjugate (Sigma). Immune complexes were washed, separated by SDS−polyacrylamide gel electrophoresis (PAGE) (6% polyacrylamide gel), and transferred to a NitroBond membrane (Osmonics, Westborough, MA). The membranes were then probed with the gp120-specific monoclonal antibody (mAb) Chessie B13 (kindly provided by G. Lewis) (*50*) and visualized by chemiluminescence with ECL-Plus (Amersham Pharmacia Biotech). Western blots were quantitated on a Fuji fluorescence imaging system (FLA3000G analyzer).

To detect cell surface-associated gp120, cell monolayers were surface-biotinylated with NHS-LC-biotin (Pierce Chemical) (*48*), and cells were then lysed on ice in 50 mM Tris-HCl (pH 7.5), 150 mM NaCl, and 1% Triton X-100 containing 1 μg/mL aprotinin, 1 μg/mL leupeptin, and 1 μg/mL pepstatin. The biotinylated envelope glycoprotein was isolated by immunoprecipitation using HIVIG, separated by SDS−PAGE (6% polyacrylamide gel), and probed by using a NeutrAvidin−horseradish peroxidase conjugate (NeutrAvidin−HRP) (Pierce Chemical) and ECL-Plus as described above. For the analysis of deglycosylated envelope polypeptides, biotinylated cell-surface proteins were isolated by using a NeutrAvidin−agarose conjugate (Pierce Chemical). The glycoproteins were deglycosylated with *N*-glycanase F (New England Biolabs, Beverly, MA), resolved by SDS−PAGE (8% polyacrylamide gel), and subjected to Western blot analysis with the gp120-specific mAb Chessie 12 (kindly provided by G. Lewis) (*50*).

Cell−Cell Fusion Assay. Mutant or wild-type envelope glycoproteins were transiently expressed in COS-7 cells and assessed for fusion activity as previously described (*48*). In the present modification of the procedure, 6×10^3 transfected COS-7 cells were plated into 96-well microcultures and 8×10^3 U87-CD4-CXCR4 cells were added the next day. Cocultures were fixed after 5 and 24 h and immunochemically stained to identify envelope glycoprotein-expressing cells. The number of syncytia was determined microscopically.

RESULTS

Alanine Core Mutants of N34(L6)C28. In the recombinant N34(L6)C28 peptide model of the gp41 ectodomain core, three C28 helices are packed into conserved, hydrophobic grooves on the surface of the N34 trimeric coiled coil (Figure 1) (*15*, *51*). Eight residues at the *a* and *d* positions of the C28 helix (Trp628, Trp631, Ile635, Tyr638, Ile642, Leu645, Ser649, and Gln652) insert into each of these grooves and make extensive hydrophobic contacts. Here we used alanine-scanning mutagenesis to determine the importance of these amino acid side chains in interhelical packing interactions in the gp41 core. In this approach, individual residues are changed to alanine (*52*). Because alanine has a relatively low hydrophobicity and the highest helix propensity of all amino acid side chains in coiled coils (*53*), we reasoned that alanine mutations would be useful probes for identifying the determinants of helix−helix interactions (*48*). The wild-type and mutant peptides were produced by bacterial expression, and the alanine mutants were named by the positions of their substitutions.

Biophysical Analysis of Mutant N34(L6)C28 Peptides. The helical content and thermal stability of mutant N34(L6)C28 peptides were quantitated by circular dichroism. Alanine

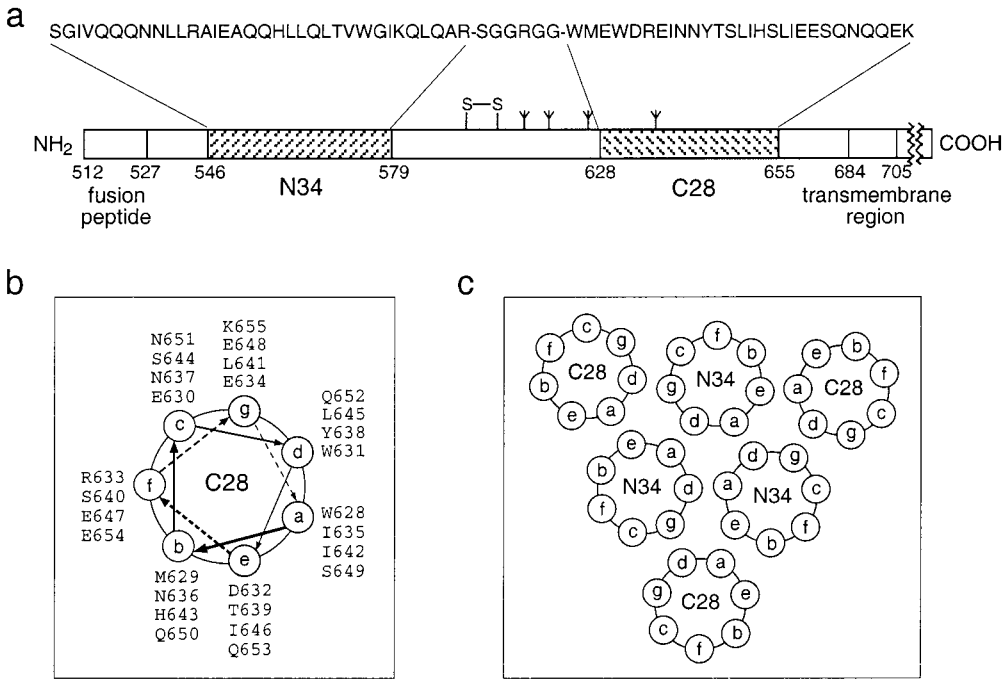

FIGURE 1: HIV-1 gp41 structure. (a) A schematic view of HIV-1 HXB2 gp41 showing important functional features, including the disulfide bond and four potential N-glycosylation sites. Regions corresponding to the N34 and C28 peptides identified by protein dissection are indicated, along with their sequences. The recombinant N34(L6)C28 protein consists of the N34 and C28 segments that are connected via a short peptide linker in place of the disulfide-bonded loop region. (b) Helical wheel projection of the C28 sequence. The *a*−*g* positions represent sequential positions in the 4,3-hydrophobic heptad repeat in the C28 sequence. The view is from the NH_2 terminus. (c) Helical wheel representation of the six-helix bundle in the gp41 ectodomain. Three inner N34 helices and three outer C28 helices are represented by circles, with heptad-repeat positions labeled *a*−*f*. Residues at the *a* and *d* positions of the C28 helices pack in an antiparallel orientation against residues at the *e* and *g* positions of the adjacent N34 helices, respectively.

Table 1: Biophysical Data of Alanine Mutants of the gp41 Core

	$[\theta]_{222}$[a] (deg cm^2 dmol^{-1})	T_m[a] (°C)	M_{obs}/M_{calc}[b]
N34(L6)C28	−31300	70	3.1
W628A	−31500	56	3.1
W631A	−24700	38	ND[c]
I635A	−31200	57	3.0
Y638A	−31300	65	3.0
I642A	−31600	61	3.1
L645A	−31800	60	3.1
S649A	−32300	76	3.1
Q652A	−32500	73	3.0

[a] All circular dichroism scans and melts were performed on 10 μM peptide solutions in PBS (pH 7.0). The circular dichroism signal at 222 nm ($[\theta]_{222\ nm}$) is reported. The midpoint of thermal denaturation (T_m) was estimated from the thermal dependence of $[\theta]_{222}$. [b] Sedimentation equilibrium results are reported as a ratio of the experimental molecular weight to the calculated molecular weight for a monomer (M_{obs}/M_{calc}). [c] Aggregated, as determined by sedimentation equilibrium.

mutations at either of the two polar residues (Ser649 or Gln652) showed stabilization of N34(L6)C28 complexes with an apparent elevation of the melting temperature (T_m) relative to that of the wild type (the change in thermal stability, ΔT_m, = 6 and 3 °C, respectively) (Table 1 and Figure 2a). Sedimentation equilibrium measurements indicated that both S649A and Q652A sedimented as discrete trimers (Table 1). The stabilizing effects observed for the alanine substitutions indicate that the buried polar residues Ser649 and Gln652 contribute unfavorably to the stability of the gp41 core (*54*). In contrast, alanine mutations of any of the six hydrophobic residues resulted in substantial destabilization of the N34(L6)C28 complex; the apparent T_m's of W628A, W631A, I635A, Y638A, I642A, and L645A were 56, 38, 57, 65, 61, and 60 °C, respectively, as compared to a value of 70 °C for the wild-type peptide (Figure 2a and Table 1). The greatest destabilization was observed with the W631A mutant ($\Delta T_m = -32$ °C). W631A also exhibited markedly decreased mean residue ellipticity at 222 nm (θ_{222}, a measure of helical content), while the five other alanine mutations had little effect on the absolute value of θ_{222} (Table 1). Like the other alanine mutants, W631A was trimeric in solution, with no systematic dependence of molecular weight on concentration between 10 and 100 μM (Figure 2b,c and Table 1). However, a systematic trend was observed in the residuals between the data for W631A and the linear fit (Figure 2c), suggesting that the peptide is prone to aggregation. Collectively, these results demonstrate that C28 residues making hydrophobic contacts with the N34 coiled-coil groove are important for stabilizing the fusogenic six-helix bundle structure of the gp41 core.

Determination of Crystal Structures of I635A and I642A. Our biophysical analysis suggests that substituting a single alanine for bulky hydrophobic residues at the *a* or *d* position of the C28 helix results in the formation of a cavity at the packing interface between the N34 coiled coil and the C28 helix and thus causes a decrease in the thermal stability of the trimeric N34(L6)C28 complex. To understand how these cavity-creating substitutions affect the conformation and stability of the gp41 core, we used X-ray crystallography to determine the structures of the I635A and I642A complexes at 1.75 and 1.88 Å resolution, respectively. We were unable to crystallize the W628A and W631A mutants. The I635A and I642A peptides were selected, in part, because an Ile → Ala substitution at either of these positions significantly destabilized the six-helix bundle structure and blocked the ability of the envelope glycoprotein to mediate cell fusion

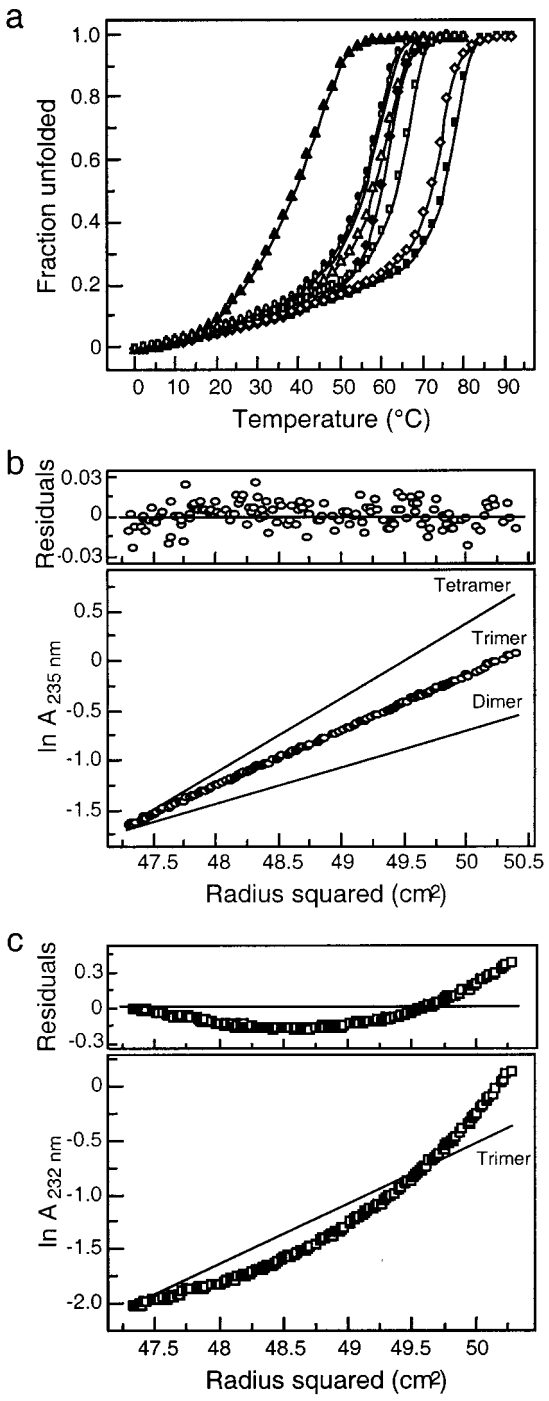

FIGURE 2: Biophysical properties of alanine mutants of N34(L6)-C28. (a) Thermal melts of W628A (●), W631A (▲), I635A (○), Y638A (□), I642A (◆), L645A (△), S649A (■), and Q652A (◇) monitored by circular dichroism at 222 nm at a protein concentration of 10 μM in PBS (pH 7.0). The decrease in the fraction of a folded molecule is shown as a function of temperature. (b) Representative equilibrium sedimentation data of a 10 μM solution of W628A at 20 °C in PBS (pH 7.0). The natural logarithm of absorbance at 235 nm is plotted against the square of the radius from the axis of rotation. The slope of the data as plotted is proportional to the molecular mass of the peptide oligomer. Lines indicate the expected slopes for dimeric, trimeric, and tetrameric states. The deviation in the data from the linear fit for a trimer model is plotted (top panel). (c) Representative equilibrium sedimentation data of a 10 μM solution of W631A at 20 °C in PBS (pH 7.0). The natural logarithm of absorbance at 232 nm is plotted against the square of the radius from the axis of rotation. Data fit closely to a trimer model, but with systematic residuals.

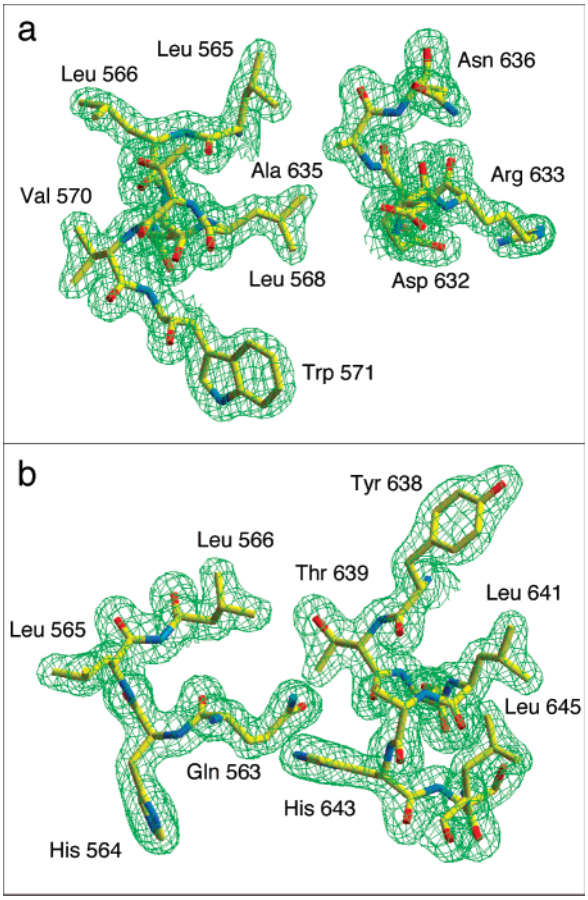

FIGURE 3: Experimental electron density maps at the substitution sites. (a) A portion of the final $2F_{obs} - F_{calc}$ map of I635A with the refined model superimposed. (b) A portion of the final $2F_{obs} - F_{calc}$ map of I642A with the refined model superimposed. The maps of I635A and I642A are contoured at 1.5σ. This figure was generated with the program SETOR (*77*).

(see below). The crystals of I635A and I642A belong to space group *R*3 and contain a monomer in the asymmetric unit, with the trimer formed around the crystallographic 3-fold axis. Both the structures were determined by a molecular replacement approach (*42*). In each case, the final $2F_{obs} - F_{calc}$ electron density map and simulated annealing omit map are readily interpretable except for a few disordered residues at the helix termini and in the short peptide linker region. Representative examples of the final $2F_{obs} - F_{calc}$ maps with the refined molecular models superimposed are shown in Figure 3. The I635A structure was refined against 25.0−1.75 Å resolution data to yield a conventional and free *R* factors of 20.6 and 22.6%, respectively. The I642A structure was refined to a conventional *R* factor of 19.7%, with a free *R* factor of 21.6% over a resolution range of 26.0−1.88 Å. Crystallographic details and results are summarized in Materials and Methods and in Table 2.

Effects of the Ile → Ala Mutations on the Hairpin Structure. The overall structures of the I635A and I642A trimers are very similar to that of the wild-type N34(L6)-C28 complex. In all cases, three hairpin-like molecules pack on the crystallographic 3-fold symmetry axis to form a six-helix bundle (Figure 4a). The inner N34 helices form a parallel, three-stranded coiled coil. The core residues at the *a* and *d* positions of the N34 peptide exhibit "acute knobs-into-hole" side chain packing characteristic of three-stranded

Table 2: X-ray Data Collection and Refinement Statistics

	I635A	I642A
data statistics		
space group	*R*3	*R*3
$a = b$, c (Å)	51.85, 60.70	52.21, 60.90
resolution (Å)	50.0−1.75	50.0−1.88
no. of reflections	36268	27873
no. of unique reflections	6132	5047
redundancy	25.4 (11.3)[a]	20.3 (11.0)[a]
I/σ(I)	44.5 (5.7)[a]	44.7 (5.0)[a]
completeness (%)	99.4	100
R_{sym} (%)[b]	3.9	3.9
refinement statistics		
resolution (Å)	25.0−1.75	26.0−1.88
no. of reflections	6132	4977
R_{cryst} (%)[c]/R_{free} (%)[d]	20.6/22.6	19.7/21.6
no. of protein non-hydrogen atoms	489	482
no. of water molecules	67	74
rms deviations		
bond lengths (Å)	0.004	0.005
bond angles (deg)	0.8	0.8
torsion angles (deg)	14.2	14.2
average *B* factor (Å^2)	32.7	31.1

[a] Values in parentheses are for the highest-resolution shell (1.81−1.75 Å for I635A and 1.95−1.88 Å for I642A). [b] $R_{sym} = \sum|I_{hi} - \langle I_h\rangle|/\sum I_{hi}$ for all h, where I_h is the intensity of reflection h. [c] $R_{cryst} = \sum||F_{obs}| - |F_{calc}||/\sum|F_{obs}|$. No σ cutoff was applied. [d] $R_{free} = \sum||F_{obs}| - |F_{calc}||/\sum|F_{obs}|$ for 10% of the reflections not used in refinement.

coiled coils (*55*, *56*). Interactions between these residues and their counterparts from the other two N34 peptides of the trimer are maintained in nine successive *a* and *d* layers perpendicular to the 3-fold axis. The outer C28 helices adopt a left-handed superhelical twist and make contacts along three hydrophobic grooves between the neighboring inner N34 helices (Figure 4b,c). The grooves are formed by highly conserved residues at the *e* and *g* positions of the N34 helix. Side chains of the *a* and *d* residues of the C28 helix are tucked into the center of the groove between two adjacent N34 helices. In I635A and I642A, both alanine replacements are in position *a* of the C28 helix. In each case, the alanine mutation is accommodated well in the six-helix bundle structure by using different sets of atoms. The wild-type and mutant structures can be superimposed, with root-mean-square (rms) differences of 0.73 Å for I635A and 0.68 Å for I642A. Thus, alanine substitutions at the conserved Ile635 and Ile642 residues each do not affect the overall conformation of the fusogenic gp41 ectodomain core.

Each hydrophobic groove on the surface of the N34 coiled coil has a deep pocket that has been proposed as an attractive drug target (*30*−*32*). This pocket is formed by residues, including amino acids Leu568, Trp571, and Lys574, on the inner N34 helix, and accommodates residues Trp628, Trp631, and Ile635 on the outer C28 helix. In the I635A crystal structure, the methyl group of the substituted Ala635 side chain docks into the hydrophobic pocket without significantly altering the six-helix bundle structure (Figure 4b). The small alanine side chain decreases the extent of favorable hydrophobic interactions in the interhelical interface and thus the gp41 core stability, as suggested by the reduction in T_m of I635A relative to that of the wild-type core.

In the I642A crystal structure, Ala642 packs into the N34 coiled-coil groove through hydrophobic contacts with the Gln563 and Leu565 residues (Figure 4c). This hydrophobic effect buries 46 Å^2 of solvent-accessible surface area. In the wild-type N34(L6)C28 structure, Ile642 interacts similarly with the coiled-coil core, with a buried surface area of 110 Å^2. Removal of three methylene groups by the Ile-to-Ala substitution creates a cavity at the tightly packed interhelical interface and thus destabilizes the six-helix bundle structure. Our biophysical and crystallographic studies indicate that the favorable van der Waals and hydrophobic interactions between the *a* and *d* residues of the C28 helix and the *e* and *g* residues of the N34 coiled coil are a dominant factor in the stabilization of the gp41 ectodomain core.

Expression of Mutant Envelope Glycoproteins. Alanine mutations were introduced into the HXB2 *env* gene by site-directed mutagenesis, and the mutant envelope glycoproteins were expressed by transient transfection in COS-7 cells. All envelope glycoprotein-expressing plasmids displayed similar transfection efficiencies. The levels of envelope glycoprotein expression, as determined by immunochemical staining and by Western blot analysis, were very similar among all alanine mutants and the wild type (Table 3). In all cases, gp120 was shed from the cell-surface envelope glycoprotein complexes. One experiment is shown in Figure 5a, and the consensus findings from multiple such experiments are summarized in Table 3. In general, the extent of gp120 shedding to the cell culture supernatant was comparable for the wild-type and mutant envelope glycoproteins. Some variability was observed between experiments, but only the Y638A mutant distinguished itself by consistently yielding >2-fold higher levels of shed gp120.

To further assess the biosynthesis of the mutant envelope glycoproteins, cell-surface proteins were biotinylated and the envelope glycoprotein was immunoprecipitated from cell lysates using HIVIG, an immunoglobulin preparation from HIV-infected persons. The cell-surface envelope glycoprotein was detected by Western blot analysis using a Neutra-Avidin−horseradish peroxidase conjugate and fluorescence imaging. Strikingly, we were unable to detect significant accumulation of gp120 on the surface of cells expressing the W628A, W631A, I635A, and I642A envelope glycoproteins (Figure 5b and Table 3). Cells expressing the other mutant envelope glycoproteins typically displayed levels of cell-surface gp120 that were similar to that of the wild type. A control, cleavage-defective envelope glycoprotein (*57*) produced only gp160. Uncleaved gp160 precursor was also found on the surface of cells expressing the mutant and wild-type envelope glycoproteins. This incomplete processing is likely due to saturation of the furin-like proteases that are responsible for the proteolytic cleavage of gp160 (*58*). In many experiments, we observed a slight reduction in the relative amount of gp160 precursor in the Y638A mutant. In conjunction with the parallel increase in the level of gp120 shedding by this mutant, these data may indicate enhanced proteolytic processing of the Y639A envelope precursor.

The apparent lack of accumulation of gp120 on the surface of cells expressing the W628A, W631A, I635A, and I642A mutants was further analyzed by enzymatic deglycosylation. Biotinylated and deglycosylated gp120 (p120) migrates as a discrete polypeptide band of approximately 55 kDa and was observed from all mutant and wild-type envelope glycoproteins, except those of the W628A, W631A, I635A, and I642A mutants (Figure 5c). These results confirm the significant absence of gp120 accumulation within the envelope glycoprotein complex of these alanine mutant

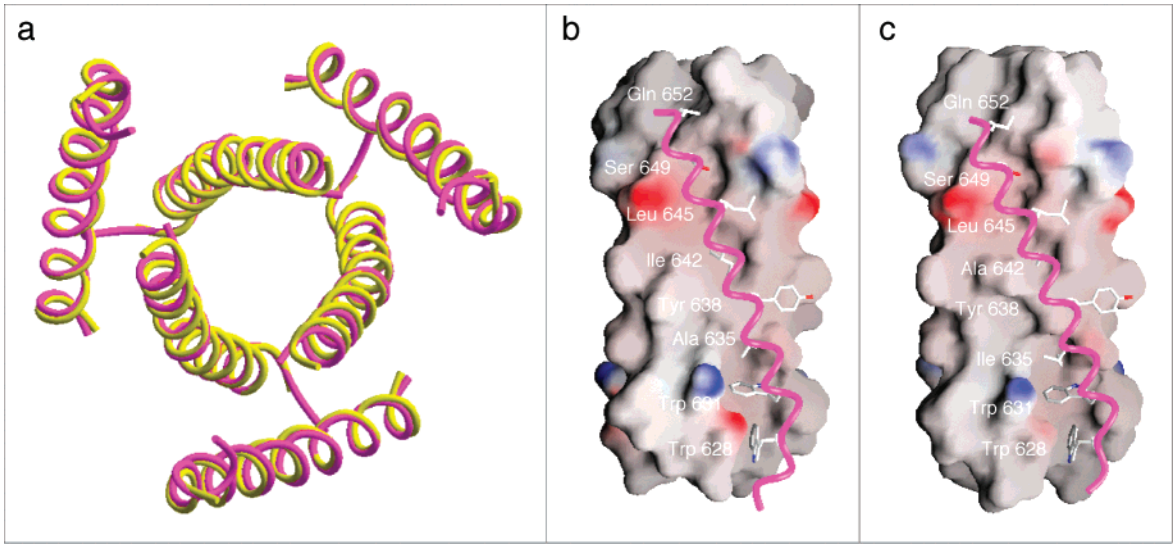

FIGURE 4: Crystal structures of the I635A and I642A trimers. (a) Top view of the superposition of the backbone traces for I635A in magenta and I642A in yellow, looking down the 3-fold axis from the loop region. (b) Helical packing interactions in I635A. The N34 coiled coil is represented as a molecular surface, and the C28 helix (magenta) is shown as a ribbon with *a* and *d* side chains (white) that pack into a hydrophobic groove on the coiled-coil surface. The NH_2 termini of the N34 helices point toward the bottom of the page, and those of the C28 helices point toward the top. (c) Helical packing interactions in I642A. The C28 helix (magenta), represented as a ribbon, is shown against a surface representation of the central N34 coiled coil. This figure was prepared with the program GRASP (*78*).

Table 3: Summary of Envelope Glycoprotein Expression and Function

	envelope protein expression[a]	cell-surface gp120[b]	gp120 shedding[c]	cell−cell fusion[d]
wild type	++	++	++	++
W628A	++	−	++	−
W631A	++	−	++	−
I635A	++	−	++	−
Y638A	++	++	+++	++
I642A	++	−	++	−
L645A	++	++	++	++
S649A	++	++	++	++
Q652A	++	++	++	++

[a] ++, mutant envelope glycoprotein expression levels comparable to the wild-type level (50−200%). [b] The steady-state levels of cell-surface gp120 and gp160 were compared. ++, gp120/gp160 ratios comparable to that of the wild type (50−200%); −, little or no cell-surface gp120 detected. [c] +++, gp120 accumulation in the cell culture supernatant is greater than 200% of that of the wild type; ++, gp120 accumulation comparable to that of the wild type (50−200%). [d] ++, fusion activity comparable to that of the wild type (50−200%); −, no syncytium formation.

glycoproteins. In the case of W628A and W631A, we often observed a smear of envelope polypeptide that migrated faster than p120 (Figure 5c), suggesting aberrant cleavage of the mutant gp160 precursor. At present, we cannot determine whether the apparent absence of intact gp120 on the surface of cells expressing the W628A, W631A, I635A, and I642A mutant glycoproteins reflects a marked reduction in the efficiency of gp160 proteolytic cleavage and/or an alteration in the stability of the gp120−gp41 association, resulting in a marked increase in the level of gp120 shedding.

Fusogenicity of Mutant Envelope Glycoproteins. We have demonstrated that single alanine substitutions at the six hydrophobic positions within the buried face of the C28 helix destabilize the gp41 core structure. Four of these mutations also result in cell-surface envelope glycoprotein complexes that are largely devoid of intact gp120. To determine the effects of these alanine mutations on the ability of the envelope glycoprotein to mediate membrane fusion, we cocultured the envelope glycoprotein-expressing cells with

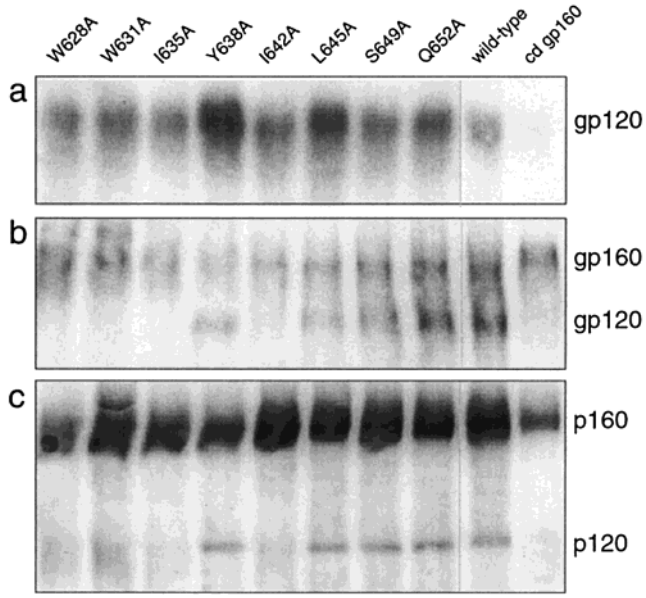

FIGURE 5: Synthesis and processing of mutant and wild-type envelope glycoproteins. (a) COS-7 cells were transfected with plasmids expressing either the wild-type or a mutant envelope glycoprotein; 48 h posttransfection, the cell culture supernatants were immunoprecipitated with HIVIG, and shed gp120 was analyzed by Western blot using the gp120-specific mAb Chessie B13. (b) Cell-surface expression of the wild-type and mutant envelope glycoproteins. Two days after transfection, the cells were labeled with NHS-LC-biotin as described in Materials and Methods. Cell lysates were prepared and immunoprecipitated with HIVIG, and cell-surface gp160 and gp120 were detected using the NeutrAvidin−HRP conjugate. (c) Analysis of deglycosylated cell-surface envelope glycoproteins. Biotinylated proteins were isolated with the NeutrAvidin−agarose conjugate and deglycosylated using *N*-glycanase F. Envelope glycoproteins were detected by Western blot analysis with the gp120-specific mAb Chessie 12. Wild-type and cleavage-defective (cd) envelope glycoproteins (gp120 and gp160) and the corresponding deglycosylated polypeptides (p120 and p160) are shown at the right.

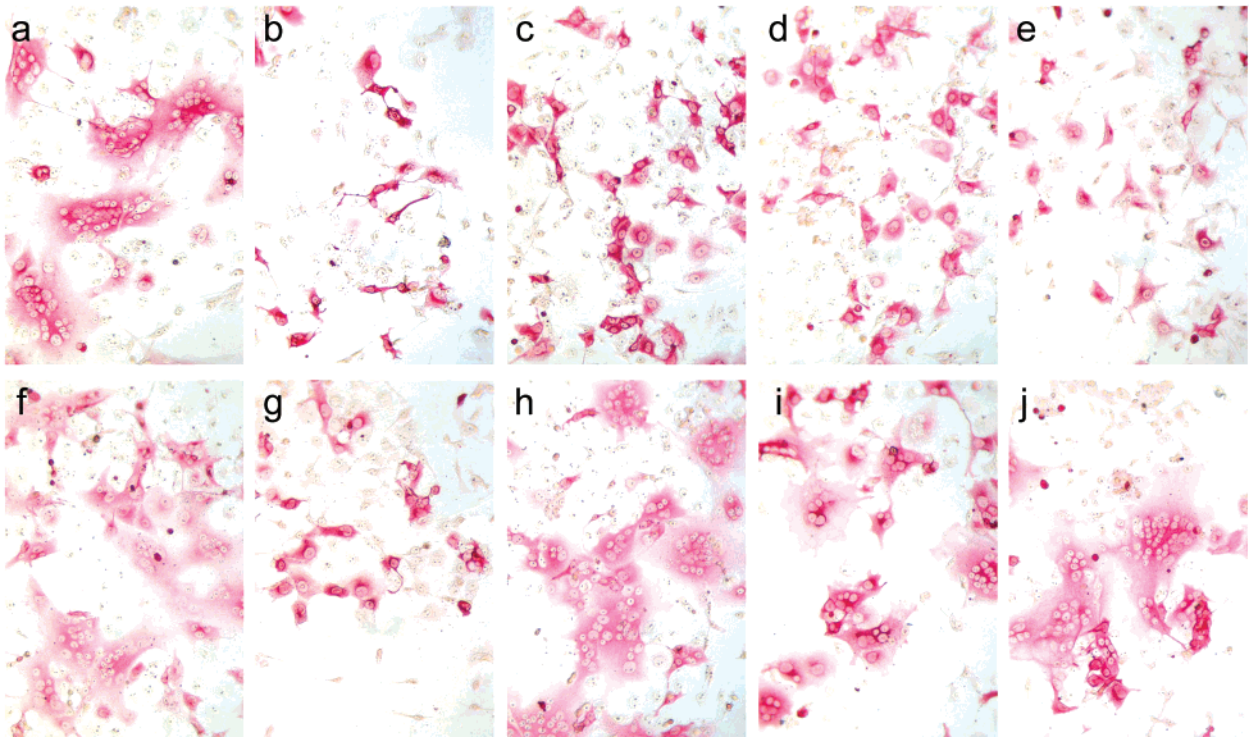

FIGURE 6: Syncytium formation by mutant envelope glycoproteins. COS-7 cells were transfected with plasmids expressing the wild-type or mutant envelope glycoproteins. Two days after transfection, U87-CD4-CXCR4 cells were added to the cultures to determine the ability of the envelope glycoproteins to mediate cell−cell fusion. Cocultures were washed and fixed after 5 h, and were immunochemically stained to identify envelope glycoprotein-expressing cells and syncytia: (a) wild type, (b) cleavage-defective envelope glycoprotein, (c) W628A, (d) W631A, (e) I635A, (f) Y638A, (g) I642A, (h) L645A, (i) S649A, and (j) Q652A. All microphotographs were taken using a 10× objective lens.

a CD4- and CXCR4-bearing fusion partner, U87-CD4-CXCR4 cells (*59*). As shown in Figure 6, syncytium formation by the Y638A, L645A, S649A, and Q652A mutant envelope glycoproteins proceeded rapidly, and after the cells had been cocultured for 5 h, the syncytia were indistinguishable in number and extent from those induced by the wild-type glycoprotein (Table 3). In contrast, syncytium formation was entirely absent in cells expressing the W628A, W631A, I635A, and I642A glycoproteins, even after the cells had been cocultured for 24 h. The control, cleavage-defective envelope glycoprotein likewise did not induce syncytia. The basis for the fusion defect in these alanine mutants is, however, more complex than in the cleavage-defective envelope glycoprotein. Although the alanine mutants do not accumulate significant levels of intact gp120 on the cell surface, they do appear to shed gp120 into the cell culture supernatant (Figure 5a). Other effects, in addition to that on the steady-state level of gp120, may also contribute to the fusion-defective phenotype of the W628A, W631A, I635A, and I642A envelope glycoproteins.

DISCUSSION

The critical importance of trimer-of-hairpins formation for HIV-1 membrane fusion activity leads to the hypothesis that interhelical packing interactions within the gp41 ectodomain core are key determinants for viral entry and its inhibition (*29*, *33*, *48*, *60*). The N34 coiled-coil surface contains three symmetry-related hydrophobic grooves that are the sites for interaction with the C28 helix (*13*−*15*). In general, the *e* and *g* residues of the N34 helix that line these grooves pack against residues at the *a* and *d* positions of the C28 helix, although additional interhelical contacts at other positions are also observed. Sequence comparisons between HIV-1 and SIV gp41 show that the residues at these contact positions are highly conserved. To better understand the structure−function relationship for the amino acid residues at the interhelical interface, we have utilized alanine-scanning mutagenesis to compare the effects of individual side chains at the eight *a* and *d* positions of the C28 helix on the conformational stability of the fusogenic gp41 core and on the membrane fusion activity of the gp120−gp41 complex. Physical biochemical studies indicate that the six-helix bundle structure of the gp41 core is destabilized by alanine substitutions at the bulky hydrophobic positions Trp628, Trp631, Ile635, Tyr638, Ile642, and Leu645. Crystal structures of the I635A and I642A mutant cores suggest that this destabilization is caused by formation of a cavity in the interhelical interface. In contrast, the substitution of polar residue Ser649 or Gln652 with alanine is stabilizing. Thus, hydrophobic interactions involving packing of apolar side chains at the buried face of the C28 helix contribute significantly to the gp41 core stability.

Our analysis of the mutant envelope glycoproteins indicates that alanine substitutions at Trp628, Trp631, Ile635, and Ile642 also appear to affect gp120−gp41 association and/or gp160 processing. In these mutants, the gp120 subunit does not accumulate within the cell-surface envelope complex. Our data do not allow us to determine whether the alanine substitutions affect proteolytic processing of the gp160 precursor and/or the noncovalent association between the gp120 and gp41 subunits. As expected, these alanine mutations abrogated envelope-mediated cell−cell fusion. In contrast, alanine mutations at Tyr638, Leu645, Ser649, and

Gln652 have little or no effect on envelope glycoprotein synthesis, transport, processing, and function. These biological results can be reconciled with the suggestion that the effects of the alanine mutations of the C28 helix on the structure and function of the envelope glycoprotein are position-dependent. Those near the amino terminus (W628A, W631A, I635A, and I642A) disrupted the surface expression of the gp120−gp41 complex and thus resulted in mutant envelope glycoproteins that are unable to mediate cell−cell fusion, whereas those (L645A, S649A, and Q652A) at the C-terminal end of the helix do not affect gp120−gp41 association and thereby fusion activity. Our studies demonstrate that the N-terminal half of the gp41 C-helix is a critical component of the HIV-1 fusion process.

A wealth of structural and functional information about the gp41-mediated membrane fusion process indicates that formation of the trimer of hairpins is intimately associated with fusion of the viral and cellular membranes during virus binding and entry (reviewed in refs *7* and *8*, and references therein). Current knowledge suggests that formation of the helical-hairpin complex can provide a ready source of energy for overcoming the activation energy barrier needed to bring two lipid bilayers into close approximation at the fusion site (*23*, *54*, *60*, *61*). According to this idea, the conformational stability of the fusogenic gp41 core is likely to be critical in determining the membrane fusion properties of the envelope glycoprotein, a notion that has been supported by previous mutagenesis studies (*48*, *60*, *61*). For instance, the Gln652 → Leu mutation at an *a* position of the C28 helix has been shown to stabilize the six-helix bundle structure and to increase HIV-1 infectivity (*29*, *62*). In our previous alanine-scanning analysis of the individual *e* and *g* residues of the N34 coiled coil, we have observed a general correlation between the thermal stability of the six-helix bundle and the fusion activity of the gp120−gp41 complex (*48*). In general, however, the dependence of membrane fusion activity on the thermal stability of the gp41 core is less apparent in these C28 mutants than in our previously characterized N34 mutants (*48*). This difference may be related to the proposal that the N34 trimeric coiled coil is formed at an earlier step of the gp41 refolding process (*51*), prior to the packing interactions between the C28 helix and the N34 coiled coil present in the fusion-active hairpin structure (refs *7* and *8*, and references therein).

The Trp628, Trp631, and Ile635 residues of the C28 peptide are inserted into a prominent hydrophobic pocket on the surface of the N34 coiled coil in the gp41 core. This hydrophobic pocket has previously been identified as an important target for antiviral drug development (*30*−*32*). Replacement of these hydrophobic residues with alanine results in marked destabilization of the gp41 core (Table 1 and ref *33*). Interestingly, the Leu565, Val570, and Gly572 residues within the N34 region that are involved in the formation of this pocket were also found to be crucial for gp41 core stability and envelope glycoprotein activity (*48*). In addition, the envelope glycoprotein bearing the Gly572 → Ala mutation fails to retain gp120 in the cell-surface envelope complex (*48*). These cavity-forming and cavity-binding residues in the N34 and C28 helices lie adjacent to the disulfide-bonded loop region of the gp41 ectodomain. This disulfide-bonded loop region is thought to act as a hinge in the formation of the trimer-of-hairpins structure. It is also an important site for gp41 interaction with the gp120 subunit within the native envelope glycoprotein complex (*58*, *63*, *64*). It would thus appear that helix-packing interactions at or near this hinge region are crucial for gp41 activation during the fusion process. Alterations within and proximal to the disulfide-bonded loop region are likely to affect the conformation and/or dynamics of the native gp120−gp41 complex.

It is possible that the increased level of gp120 shedding we observed in the Y638A envelope glycoprotein may reflect destabilization of the native gp120−gp41 complex, as well as a potential increase in the proteolytic cleavage of gp160. Similarly, mutations that result in the apparent absence of intact gp120 within the envelope glycoprotein complex (Trp628, Trp631, Ile635, and Ile642 in the C28 helix and Gly572 and Arg579 in the N34 helix) may also alter the native envelope glycoprotein conformation through this putative gp120−gp41 interface. It has been proposed that an immune response to the native envelope glycoprotein complex may lead to the production of neutralizing antibodies (*65*−*68*). A major problem in the development of vaccines based on the HIV-1 envelope glycoprotein is the instability of the gp120−gp41 complex (*69*−*72*). Attempts to stabilize the native envelope glycoprotein structure have to date relied on approaches to incorporating disulfide bonds between the gp41 ectodomain or between the gp120 and gp41 subunits (*73*−*76*). Mutations that stabilize the gp120−gp41 association could prove to be invaluable in developing stable native envelope glycoprotein immunogens.

ACKNOWLEDGMENT

We thank Xiuwen Ma for excellent technical assistance and George Lewis (Institute of Human Virology, University of Maryland, College Park, MD) for providing Chessie 12 and B13 hybridomas.

REFERENCES

1. Hunter, E., and Swanstrom, R. (1990) *Curr. Top. Microbiol. Immunol. 157*, 187−253.
2. Luciw, P. A. (1996) in *Fields Virology* (Fields, B. N., Knipe, D. M., Howley, P. M., Chanock, R. M., Melinick, J. L., Monath, T. P., Roizman, B., and Straus, S. E., Eds.) pp 1881−1952, Lippincott-Raven Publishers, Philadelphia.
3. Kwong, P. D., Wyatt, R., Robinson, J., Sweet, R. W., Sodroski, J., and Hendrickson, W. A. (1998) *Nature 393*, 648−659.
4. Rizzuto, C. D., Wyatt, R., Hernandez-Ramos, N., Sun, Y., Kwong, P. D., Hendrickson, W. A., and Sodroski, J. (1998) *Science 280*, 1949−1953.
5. Berger, E. A., Murphy, P. M., and Farber, J. M. (1999) *Annu. Rev. Immunol. 17*, 657−700.
6. Hernandez, L. D., Hoffman, L. R., Wolfsberg, T. G., and White, J. M. (1996) *Annu. Rev. Cell Dev. Biol. 12*, 627−661.
7. Weissenhorn, W., Dessen, A., Calder, L. J., Harrison, S. C., Skehel, J. J., and Wiley, D. C. (1999) *Mol. Membr. Biol. 16*, 3−9.
8. Eckert, D. M., and Kim, P. S. (2001) *Annu. Rev. Biochem. 70*, 777−810.
9. Delwart, E. J., Mosialos, G., and Gilmore, T. (1990) *AIDS Res. Hum. Retroviruses 6*, 703−706.
10. Chambers, P., Pringle, C. R., and Easton, A. J. (1990) *J. Gen. Virol. 71*, 3075−3080.
11. Gallaher, W. R., Ball, J. M., Garry, R. F., Griffin, M. C., and Montelaro, R. C. (1989) *AIDS Res. Hum. Retroviruses 5*, 431−440.
12. Lu, M., Blacklow, S. C., and Kim, P. S. (1995) *Nat. Struct. Biol. 2*, 1075−1082.
13. Chan, D. C., Fass, D., Berger, J. M., and Kim, P. S. (1997) *Cell 89*, 263−273.

14. Weissenhorn, W., Dessen, A., Harrison, S. C., Skehel, J. J., and Wiley, D. C. (1997) *J. Virol. 72*, 9676−9682.
15. Tan, K., Liu, J., Wang, J., Shen, S., and Lu, M. (1997) *Proc. Natl. Acad. Sci. U.S.A. 94*, 12303−12308.
16. Jiang, S., Lin, K., and Lu, M. (1998) *J. Virol. 72*, 10213−10217.
17. Chan, D. C., and Kim, P. S. (1998) *Cell 93*, 681−684.
18. Hughson, F. M. (1997) *Curr. Biol. 7*, R565−R569.
19. Furuta, R. A., Wild, C. T., Weng, Y., and Weiss, C. D. (1998) *Nat. Struct. Biol. 5*, 276−279.
20. Melikyan, G. B., Markosyan, R. M., Hemmati, H., Delmedico, M. K., Lambert, D. M., and Cohen, F. S. (2000) *J. Cell Biol. 151*, 413−424.
21. Jones, P. L., Korte, T., and Blumenthal, R. (1998) *J. Biol. Chem. 273*, 404−409.
22. Munoz-Barroso, I., Durell, S., Sakaguchi, K., Appella, E., and Blumenthal, R. (1998) *J. Cell Biol. 140*, 315−323.
23. Jelesarov, I., and Lu, M. (2001) *J. Mol. Biol. 307*, 637−656.
24. Wild, C. T., Oas, T., McDanal, C. B., Bolognesi, D., and Matthews, T. J. (1992) *Proc. Natl. Acad. Sci. U.S.A. 89*, 10537−10541.
25. Jiang, S., Lin, K., Strick, N., and Neurath, A. R. (1993) *Nature 365*, 113.
26. Kilby, J. M., Hopkins, S., Venetta, T. M., DiMassimo, B., Cloud, G. A., Lee, J. Y., Alldredge, Y., Hunter, E., Lambert, D., Bolognesi, D., Matthews, T., Johnson, M. R., Nowak, M. A., Shaw, G. M., and Saag, M. S. (1998) *Nat. Med. 4*, 1302−1307.
27. Chen, C. H., Matthews, T. J., McDanal, C. B., Bolognesi, D. P., and Greenberg, M. L. (1995) *J. Virol. 69*, 3771−3777.
28. Rimsky, L. T., Shugars, D. C., and Matthews, T. J. (1998) *J. Virol. 72*, 986−993.
29. Shu, W., Liu, J., Ji, H., Radigen, L., Jiang, S., and Lu, M. (2000) *Biochemistry 39*, 1634−1642.
30. Eckert, D. M., Malashkevich, V. N., Hong, L. H., Carr, P. A., and Kim, P. S. (1999) *Cell 99*, 103−115.
31. Ferrer, M., Kapoor, T. M., Strassmaier, T., Weissenhorn, W., Skehel, J. J., Oprian, D., Schreiber, S., Wiley, D. C., and Harrison, S. C. (1999) *Nat. Struct. Biol. 6*, 953−960.
32. Sodroski, J. (1999) *Cell 99*, 243−246.
33. Chan, D. C., Chutkowski, C. T., and Kim, P. S. (1998) *Proc. Natl. Acad. Sci. U.S.A. 95*, 15613−15617.
34. Kunkel, T. A., Roberts, J. D., and Zakour, R. A. (1987) *Methods Enzymol. 154*, 367−382.
35. Edelhoch, H. (1967) *Biochemistry 6*, 1948−1954.
36. Chen, Y.-H., Yang, J. T., and Chau, K. H. (1974) *Biochemistry 13*, 3350−3359.
37. Cantor, C., and Schimmel, P. (1980) *Biophysical Chemistry*, Freeman, New York.
38. Johnson, M. L., Correia, J. J., Yphantis, D. A., and Halvorson, H. R. (1981) *Biophys. J. 36*, 575−588.
39. Laue, T. M., Shah, B. D., Ridgeway, T. M., and Pelletier, S. L. (1992) in *Analytical Ultracentrifugation in Biochemistry and Polymer Science* (Harding, S. E., Rowe, A. J., and Horton, J. C., Eds.) pp 90−125, Royal Society of Chemistry, Cambridge, U.K.
40. Otwinowski, Z., and Minor, W. (1997) *Methods Enzymol. 276*, 307−326.
41. Collaborative Computational Project, No. 4 (1994) *Acta Crystallogr. D50*, 760−763.
42. Navaza, J. (1994) *Acta Crystallogr. A50*, 157−163.
43. Jones, T. A., Zou, J. W., Cowan, S. W., and Kjelgaard, M. (1991) *Acta Crystallogr. D47*, 110−119.
44. Brünger, A. T. (1992) *XPLOR Version 3.1: A System for X-ray Crystallography and NMR*, Yale University Press, New Haven, CT.
45. Brünger, A. T., Adams, P. D., Clore, G. M., DeLano, W. L., Gros, P., Grosse-Kunstleve, R. W., Jiang, J.-S., Kuszewski, J., Nilges, M., Pannu, N. S., Read, R. J., Rice, L. M., Simonson, T., and Warren, G. L. (1998) *Acta Crystallogr. D54*, 905−921.
46. Laskowski, R. A., MacArthur, M. V., Moss, D. D., and Thornton, J. M. (1993) *J. Appl. Crystallogr. 26*, 283−291.
47. LaCasse, R. A., Follis, K. E., Moudgil, T., Trahey, M., Binley, J. M., Planelles, V., Zolla-Pazner, S., and Nunberg, J. H. (1998) *J. Virol. 72*, 2491−2495.
48. Lu, M., Stoller, M. O., Wang, S., Liu, J., Fagan, M. B., and Nunberg, J. H. (2001) *J. Virol. 75*, 11146−11156.
49. Prince, A. M., Reesink, H., Pascual, D., Horowitz, B., Hewlett, I., Murthy, K. K., Cobb, K. E., and Eichberg, J. W. (1991) *AIDS Res. Hum. Retroviruses 7*, 971−973.
50. Abacioglu, Y. H., Fouts, T. R., Laman, J. D., Claassen, E., Pincus, S. H., Moore, J. P., Roby, C. A., Kamin-Lewis, R., and Lewis, G. K. (1994) *AIDS Res. Hum. Retroviruses 10*, 371−381.
51. Lu, M., Ji, H., and Shen, S. (1999) *J. Virol. 73*, 4433−4438.
52. Cunningham, B. C., and Wells, J. A. (1989) *Science 244*, 1081−1085.
53. O'Neil, K. T., and DeGrado, W. F. (1990) *Science 250*, 646−651.
54. Ji, H., Bracken, C., and Lu, M. (2000) *Biochemistry 39*, 676−685.
55. Crick, F. H. C. (1953) *Acta Crystallogr. 6*, 689−697.
56. Harbury, P. B., Kim, P. S., and Alber, T. (1994) *Nature 371*, 80−83.
57. Freed, E. O., Myers, D. J., and Risser, R. (1989) *J. Virol. 63*, 4670−4675.
58. Binley, J. M., Sanders, R. W., Clas, B., Schuelke, N., Master, A., Guo, Y., Kajumo, F., Anselma, D. J., Maddon, P. J., Olson, W. C., and Moore, J. P. (2000) *J. Virol. 74*, 627−643.
59. Hill, C. M., Deng, H., Unutmaz, D., Kewalramani, V. N., Bastiani, L., Gorny, M. K., Zolla-Pazner, S., and Littman, D. R. (1997) *J. Virol. 71*, 6296−6304.
60. Liu, J., Wang, S., Hoxie, J. A., LaBranche, C. C., and Lu, M. (2002) *J. Biol. Chem. 277*, 12891−12900.
61. Liu, J., Shu, W., Fagan, M. B., Nunberg, J. H., and Lu, M. (2001) *Biochemistry 40*, 2797−2807.
62. Cao, J., Bergeron, L., Helseth, E., Thali, M., Repke, H., and Sodroski, J. (1993) *J. Virol. 67*, 2747−2755.
63. Helseth, E., Olshevsky, U., Furman, C., and Sodroski, J. (1991) *J. Virol. 65*, 2119−2123.
64. Schultz, T. F., Jameson, B. A., Lopalco, L., Siccardi, A. G., Weiss, R. A., and Moore, J. P. (1992) *AIDS Res. Hum. Retroviruses 8*, 1585−1594.
65. Moore, J. P., and Ho, D. D. (1995) *J. Acquired Immune Defic. Syndr. 9* (Suppl. A), S117−S136.
66. Burton, D. R., and Montefiori, D. C. (1997) *J. Acquired Immune Defic. Syndr. 11* (Suppl. A), 587−598.
67. Parren, P. W. H. I., Burton, D. R., and Sattentau, Q. J. (1997) *Nat. Med. 3*, 366−367.
68. Parren, P. W. H. I., Moore, J. P., Burton, D. R., and Sattentau, Q. J. (1999) *J. Acquired Immune Defic. Syndr. 13* (Suppl. A), S137−S162.
69. Gelderblom, H. R., Reupke, H., and Pauli, G. (1985) *Lancet ii*, 1016−1017.
70. Moore, J. P., McKeating, J. A., Weiss, R. A., and Sattentau, Q. J. (1990) *Science 250*, 1139−1142.
71. McKeating, J. A., McKnight, A., and Moore, J. P. (1991) *J. Virol. 65*, 852−860.
72. Poignard, P., Fotus, T., Naniche, D., Moore, J. P., and Sattentau, Q. J. (1996) *J. Exp. Med. 183*, 473−484.
73. Farzan, M., Choe, H., Desjardins, E., Sun, Y., Kuhn, J., Cao, J., Archambault, D., Kolchinsky, P., Koch, M., Wyatt, R., and Sodroski, J. (1998) *J. Virol. 72*, 7620−7625.
74. Binley, J. M., Sanders, R. W., Clas, B., Schuelke, N., Master, A., Guo, Y., Kajumo, F., Anselma, D. J., Maddon, P. J., Olson, W. C., and Moore, J. P. (2000) *J. Virol. 74*, 627−643.
75. Yang, X., Farzan, M., Wyatt, R., and Sodroski, J. (2000) *J. Virol. 74*, 5716−5725.
76. Yang, X., Florin, L., Farzan, M., Kolchinsky, P., Kwong, P. D., Sodroski, J., and Wyatt, R. (2000) *J. Virol. 74*, 4746−4754.
77. Evans, S. V. (1993) *J. Mol. Graphics 11*, 134−138.
78. Nichols, A., Sharp, K., and Honig, B. (1991) *Proteins: Struct., Funct., Genet. 11*, 281−296.

BI025648Y